J Solid State Electrochem (2011) 15:2041–2052
DOI 10.1007/s10008-010-1221-7

ORIGINAL PAPER

Immobilization of flavine adenine dinucleotide onto nickel oxide nanostructures modified glassy carbon electrode: fabrication of highly sensitive persulfate sensor

Abollah Salimi · Abdollah Noorbakhsh · Abolfazl Semnani

Received: 8 May 2010 / Revised: 14 October 2010 / Accepted: 18 October 2010 / Published online: 9 November 2010

Abstract A simple method was used to fabricate flavin adenine dinucleotide (FAD)/NiOx nanocomposite on the surface of glassy carbon (GC) electrode. Cyclic voltammetry technique was applied for deposition nickel oxide nanostructures onto GC surface. Owing to its high biocompatibility and large surface area of nickel oxide nanomaterials with immersing the GC/NiOx-modified electrode into FAD solution for a short period of time, 10–140 s, a stable thin layer of the FAD molecules immobilized onto electrode surface. The FAD/NiOx films exhibited a pair of well-defined, stable, and nearly reversible CV peaks at wide pH range (2–10). The formal potential of adsorbed FAD onto nickel oxide nanoparticles film, $E^{o'}$ vs. Ag/AgCl reference electrode is −0.44 V in pH 7 buffer solutions was similar to dissolved FAD and changed linearly with a slope of 58.6 mV/pH in the pH range 2–10. The surface coverage and heterogeneous electron transfer rate constant (k_s) of FAD immobilized on NiOx film glassy carbon electrode are 4.66×10^{-11} mol cm^{-2} and 63± 0.1 s^{-1}, indicating the high loading ability of the nickel oxide nanoparticles and great facilitation of the electron transfer between FAD and nickel oxide nanoparticles. FAD/NiOx nanocomposite-modified GC electrode shows excellent electrocatalytic activity toward $S_2O_8^{2-}$ reduction at reduced overpotential. Furthermore, rotated modified electrode illustrates good analytical performance for amperometric detection of $S_2O_8^{2-}$. Under optimized condition, the concentration calibration range, detection limit, and sensitivity were 3 μM–1.5 mM, 0.38 μM and 16.6 nA/μM, respectively.

Keywords FAD · Nickel oxide · Nanoparticles · Glassy carbon electrode · $S_2O_8^{2-}$ · Sensor

Introduction

Flavin adenine dinucleotide (FAD) is a flavoprotein coenzyme that plays an important biological role in many oxidoreductases and in reversible redox conversions in biochemical reactions [1]. FAD and its reduced form (FADH2) have an isoalloxazine ring as the redox-active component that readily accepts and donates electrons. This makes it ideally suited to be an intermediate that is cyclically reduced and then re-oxidized by the metabolic reactions [2]. The electrochemical reaction mechanism of FAD was thoroughly studied on various electrode materials by many authors throughout a broad pH range in aqueous solution [2–6]. FAD in particular has been extensively studied on several solid electrodes such as Au [2, 7, 8], Pt [9], glassy carbon [10–12], titanium oxide [13], and pyrolytic graphite [14, 15]. Due to importance role of flavin molecules in biological systems, the investigation of electrochemical properties of electrodes modified with adsorbed flavin is important [3]. Furthermore, the direct

Electronic supplementary material The online version of this article (doi:10.1007/s10008-010-1221-7) contains supplementary material, which is available to authorized users.

A. Salimi · A. Noorbakhsh
Department of Chemistry, University of Kurdistan,
P.O. Box 416, Sanandaj, Iran

A. Salimi (✉)
Research Center for Nanotechnology, University of Kurdistan,
P.O. Box 416, Sanandaj, Iran
e-mail: absalimi@yahoo.com

A. Salimi
e-mail: absalimi@uok.ac.ir

A. Semnani
Faculty of Science, University of Shahr Kord,
Shahr Kord, Iran

electron transfer between the redox-active group and electrode can serve as a model system to aid the understanding of the electron transfer mechanisms in biological systems. In addition, the reversible direct electron transfer between adsorbed FAD and different electrode surfaces provides a basis for, sensors, biosensors, enzymatic reactors, and biomedical devices. FAD did not strongly adsorb on bare novel metals and glassy carbon electrodes [8]. Therefore, finding effective and simple procedure to immobilize FAD on electrode surfaces for the fabrication of new sensors and biosensors is essential. The electrochemical behavior and electrocatalytic activity of FAD on different modified electrode was investigated. Chen et al. [16] have reported the electrochemical properties of immobilized FAD onto nordihydroguaiaretic acid, polyluminol [17], poly (p-aminobenzene sulfonic acid) [18], and poly-diallyldimethylammonium chloride films [19]. The modified electrodes have been used for improvement the electrochemical reversibility of $NADH/NAD^+$ redox reaction and electrocatalytic reduction of oxygen and sufur oxoanions.

The combined unique properties offered by both biomolecules and inorganic nanomaterials make such nanocomposites attractive for a wide range of applications including mimetic biominerals, biomedicine, sensors, and so on [20–22]. Transition metal single and mixed oxides with electrical, magnetic, and opto-electronic properties are expected to provide novel bio-nanocomposites build up as multicomponent and multifunctional materials [23]. Based on unique properties of metal oxide, they can be used for immobilization of different biomolecules to form new bionanocomposite. Recently, glassy carbon electrodes modified with zinc oxide [1, 24], titanium oxide [3], and cobalt oxide [25] nanostructures were successfully used for immobilization and electrocatalytic application of FAD.

In the past years, the research on the synthesis of nanosized porous nickel oxide materials and its applications in catalytic reactions, industries processes, and electrochromic devices has been rather intense [26–28]. Electrochemical co-deposition of enzymes and matrix is a convenient single step, which is fast and well-controlled method [29]. Due to unique properties of nickel oxide nanostructures, they can be used for immobilization of different molecules and biomolecules to fabrication of sensors and biosensors [30–33]. The easy preparation, electroinactivity in physiological pH solutions, high porosity, and biocompatibility are advantages of nickel oxide nanomaterials for biomolecules and electron transfer mediators' entrapment. As shown in Scheme 1, FAD consists of the nucleotide adenine, the sugar ribose, and two phosphate groups. The formation of highly stable complexes between Ni^{2+} and 2′-deoxyguanosine 5′-monophosphate and triphosphate, the molecules with similar FAD structure (Scheme 1) have been reported [34, 35].The coordination of negatively charged oxygen donors(i.e., phosphate group) and N-7 of guanine ring with Ni^{2+} ion confirmed the formation of stable complex. Therefore, due to formation of stable complexes between phosphate and nitrogen of adenine group in FAD, it can be immobilized strongly on the NiOx nanomaterials. To our best knowledge, no study has been reported using nickel oxide nanostructures for immobilization FAD to fabricate sensor. Following our previous works for electrochemical detection of sulfur oxoanions [36], the electrocatalytic activity of FAD immobilized onto nickel oxide film for catalytic reduction of peroxydisulfate was evaluated.

Experimental

Chemicals and reagents

Flavin adenine dinucleotide disodium salt was purchased from Sigma and FAD solutions were prepared without further purification using double-distilled water. $Ni(NO)_2$ $Na_2S_2O_8$ and other reagents used were of analytical grade the phosphate buffer solutions (PBS; 0.1 M) were prepared form H_3PO_4, KH_2PO_4, and K_2HPO_4. The pH of buffer solutions was adjusted with HCl and KOH solutions. Pure N_2 (99.999%) was passed through the solution to avoid possible oxidation during the experiments.

Apparatus

Electrochemical experiments were performed with a computer controlled μ-Autolab modular electrochemical system (Eco Chemie Ultecht, The Netherlands), driven with GPES software (Eco Chemie). A conventional three-electrode cell was used with a Ag/AgCl (saturated; 3 M KCl) as reference electrode, a Pt wire as counter electrode and a glassy carbon disk (modified and unmodified) as working electrode. Voltammetry on electrodes coated with nickel oxide/FAD was done in buffers containing no FAD and nickel salt. All measurements were conducted in a thermostated temperature of 25±1 °C. Preparation of Nickel oxide-modified glassy carbon electrode (2 mm diameter) was carefully polished with alumina on polishing cloth. The electrode was placed in ethanol container and used bath ultrasonic cleaner in order to remove adsorbed particles. Nickel oxyhydroxide film was electrodeposited on the surface of glassy carbon electrode from 1 mM nickel–chloride pH 4 phosphate buffer solution, using repetitive potential cycling (30 cycles at 100 mVs^{-1}) between 0 and −1.1 V. The potential was repetitively cycled (30 scans) from 0 to 1 V at a scan rate of 100 mVs^{-1} in fresh phosphate solution (pH 12) for the electrodissolution and passivation of a

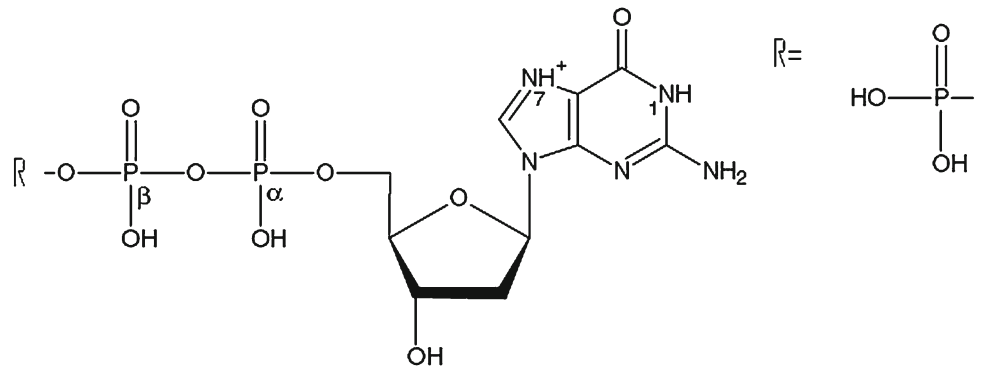

2'- deoxyguanosine 5'- triphosphate

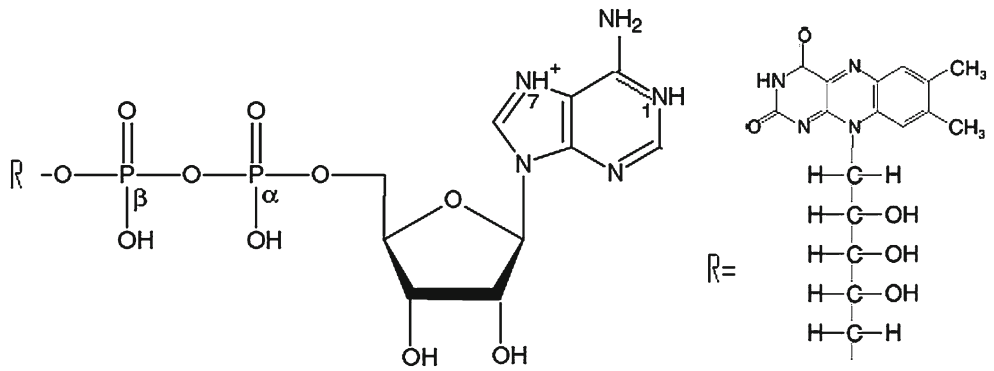

Flavine adenine dinucleotide (FAD)

Scheme 1 Molcular structures of 2′- deoxyguanosine 5'- triphosphate and flavin adenine dinucleotide (FAD)

nickel oxide layer at a GC electrode [9]. Modified electrode was eventually washed with double-distilled water and stored at ambient temperature (25 °C) before being used in experiments. Infrared spectra were obtained on a Fourier transform infrared spectroscopy (FT-IR) JASCO 680 plus spectrophotometer. Ultraviolet and visible (UV–vis) absorption spectra were recorded with a Carry 1A UV–vis spectrometer (Perkin Elmer instruments).

Immobilization of FAD onto a GC electrode modified with nickel oxide nanoparticles

Simple adsorption method was used for immobilization of FAD onto nickel oxide nanostructures. After the electrodeposition of nickel oxyhydroxide nanomaterials onto GC electrode, the electrode was immersed in fresh phosphate solution containing 1 mg ml^{-1} FAD for 20–120 s. FAD adsorbed irreversibly and strongly onto nickel oxide, due to presence of phosphate, and N-7 adenine nitrogen groups in FAD which normally have good affinity for the Ni–OH groups (Scheme 2). The electrode surface is rinsed with deionized water before using. Te same procedure was used for bare GCE in the presence FAD. The effective surface area of the electrode modified with nickel oxide nanoparticles was determined as 0.085 cm^2 from cyclic voltammogram of 1 mM K_3 $[Fe(CN)_6]$ in buffer solution pH 7. Finally, the modified electrode was removed from FAD solution, washed with double-distilled water and stored at refrigerator temperature (4 °C) before being used in experiments

Results and discussions

Surface characterization and electrochemical properties of FAD/NiOx film

The formation of nickel oxide layer on the electrode surface was checked by recording the cyclic voltammograms of the modified electrode in alkaline solution (not shown). After nickel dissolution and oxide formation in alkaline solution, the anodic and cathodic peaks at 0.48 and 0.41 V is observed, characteristic of the $Ni(OH)_2/NiO(OH)$ redox couple [37]. For bare GC electrode, no redox response was observed at potential range 0.0–0.7 V. The formation and growth of the nickel oxide nanoparticles on glassy carbon electrode was also investigated by taking atomic force microscopy (AFM) images (Fig. 1). As shown, nickel oxide

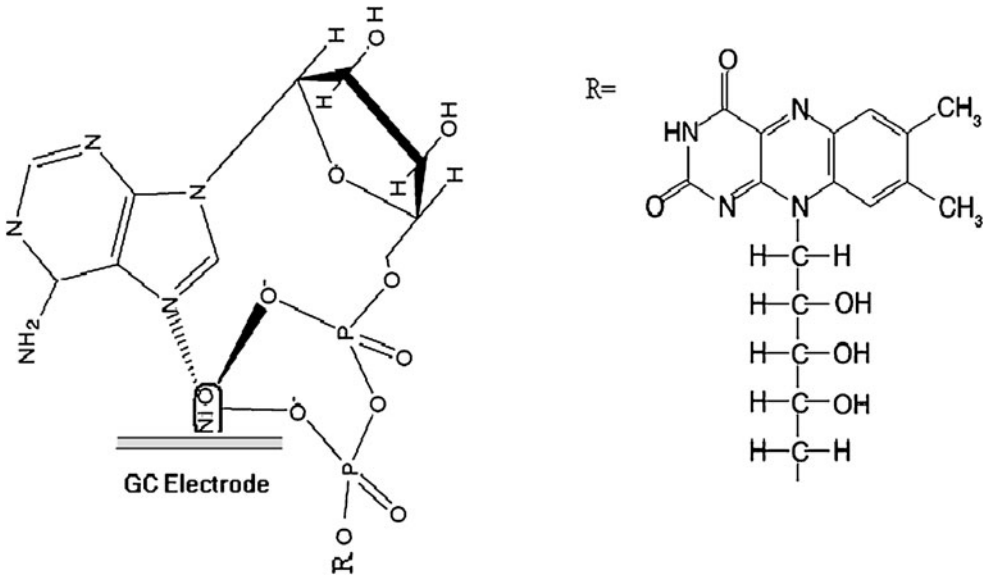

Scheme 2 Schematic representation of FAD immobilized on the nickel oxide nanoparticles modified glassy carbon electrode

particles have grown by electrodeposition on the amorphous glassy carbon surface. The AFM image also shows that the nickel oxide nanostructure with an average diameter ranging from 30 to 80 nm electrodeposited on the GC electrode. Figure 2A shows the cyclic voltammograms of NiOx and NiOx/FAD-modified GC electrodes in buffer solution (pH 7). As shown for the NiOx-modified GC electrode, no redox peaks were observed (voltammogram "a") at a potential range of −0.65 to −0.2 V, which provides a potential window of the NiOx/GC electrode for investigating the voltammetric behavior o f FAD. By immersing the GC/NiOx-modified electrode in 10 mM FAD solution for 120 s, a stable thin layer of FAD was adsorbed. As illustrated for GC electrode modified with nickel oxide/FAD, a well-defined cyclic voltammogram with a peak potential separation of less than 20 mV and a peak current of 1.3 μA was observed at a formal potential of −0.444 V (Fig. 2A voltammogram "b"). Figure 2B shows the cyclic voltammetric response of GC electrode modified with nickel oxide nanoparticles with different surface concentration of FAD, obtained by soaking the GC/NiOx electrode in 1 mg ml^{-1} FAD solution for different times at 100 mVs^{-1} in the blank solution of 0.1 M phosphate buffer (pH 7). As shown by immersing the electrode for 5 s, a stable thin layer of FAD adsorbed at the surface of electrode. By increasing the immersing time, the surface concentration of FAD is increased and starts to level off after 120 s. This result indicate that the porous interfacial layer of the nano-NiOx-modified electrode with a high specific surface area increases the conductive area, FAD can penetrate through the conductive porous channels onto the electrode more easily, leading to a higher redox response and the reversibility of FAD is significantly improved. Figure 3 demonstrates the cyclic voltammograms of a glassy carbon electrode modified with the FAD/NiOx film in PBS pH 7, at different scan rates. Figure 3C explains the plots of the anodic and cathodic peak current vs. the scan rate for the modified electrode. Both the anodic and cathodic peaks currents are linearly proportional to the scan rate in the range of 10–900 mVs^{-1}, indicating a surface-confined electrode process. Moreover, redox potentials are almost the same at the different scan rate, indicating that FAD adsorbed onto the surface undergoes a reversible electron transfer with the nickel oxide nanoparticles. The peak-to-peak separation is about 20 mV at scan rates below 100 mVs^{-1} suggesting facile charge transfer kinetics over this range of sweep rates.

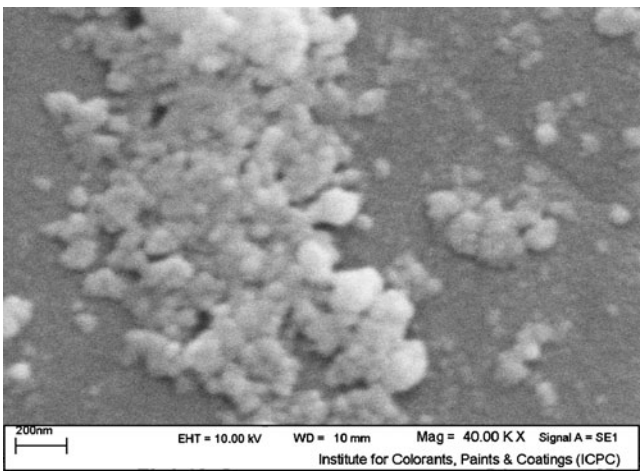

Fig. 1 SEM image of GC electrode modified with electrodeposited nickel oxide nanoparticles

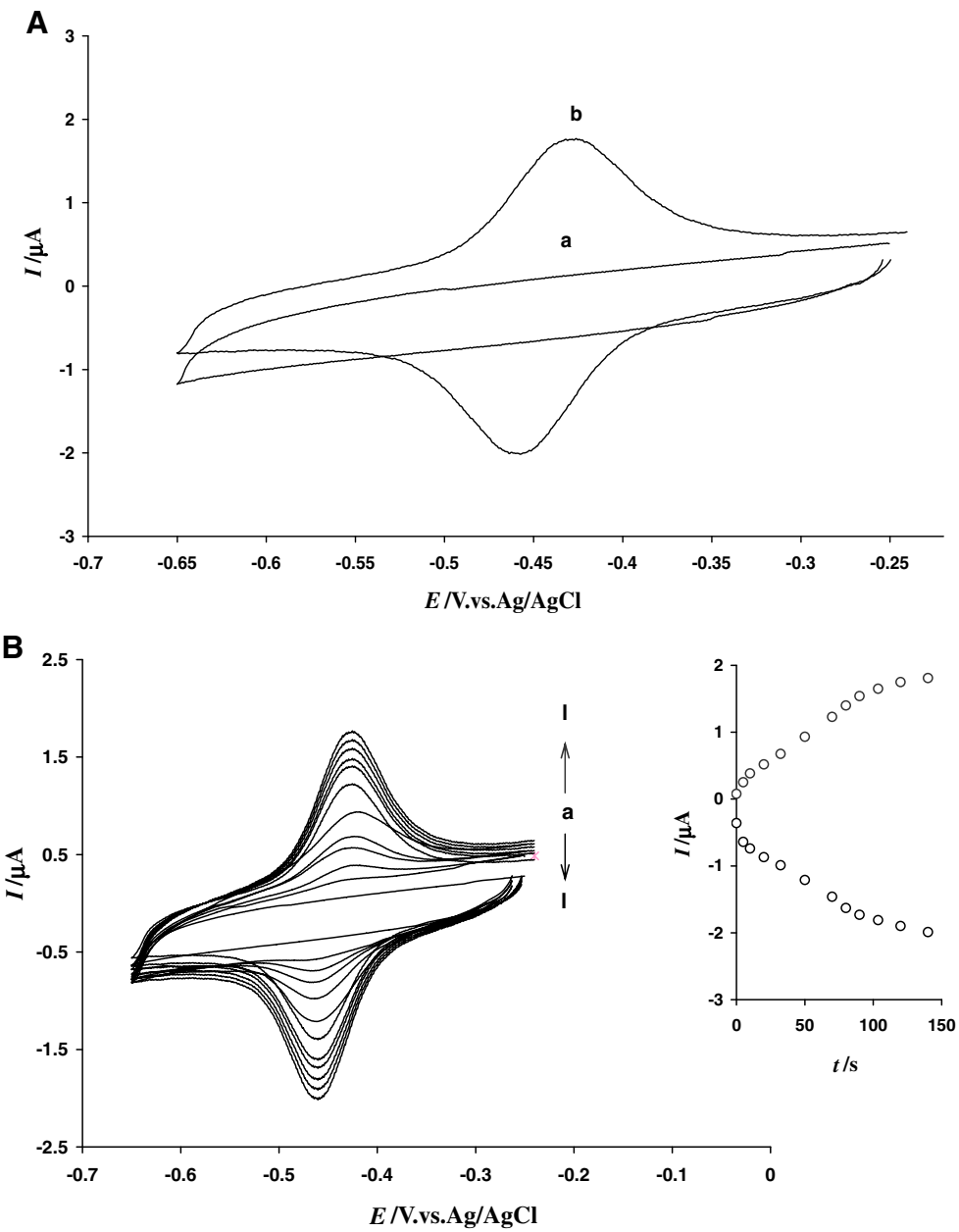

Fig. 2 (**A**) Cyclic voltamograms of NiOx nanoparticle-modified GC electrode (*a*) and NiOx/FAD-modified GC electrode (*b*) in pH 7 PBS, scan rate 100 mVs^{-1}. (**B**) Cyclic \voltammetric responses of NiOx/FAD-modified GC electrode in PBS, pH 7 at scan rate 100 mV s^{-1} modified with immersion in 1 mg ml^{-1} for different time (from inert to outer) 0, 5, 10, 20, 30, 50, 70, 80, 90, 100, 120, and 140 s. *Inset* plot of peak currents vs. immersing time

According to the slope of the Ip vs. v curve and the following equation the surface concentration (Γ_c) of FAD on the surface of nickel oxide, nanoparticles-modified GC electrode was estimated [38].

$$I_p = n^2F^2vA\Gamma_c/4RT \quad (1)$$

Where v is the sweep rate, A is the effective surface area (0.27 cm^2) of the modified electrode, and the other symbols have their usual meaning. From the slope of cathodic peak currents vs. scan rate, the calculated surface concentration of FAD is 4.66×10^{-11} mol cm^{-2}. At higher sweep rates, the plot of peak currents versus scan rate deviates from linearity and the peak current becomes proportional to the square root of the scan rate (Fig. 3D), indicating a diffusion-controlled process. The slow diffusion of counter ions (H^+) into the electrode surfaces controlled the electrochemical reaction. At higher sweep rates (v>6000 mVs^{-1}) peak separations begin to increase, indicating the limitation due to charge transfer kinetics. Based on Laviron theory [39], the electron transfer rate constant (k_s) and charge transfer coefficient (α) can be determined by measuring the variation of peak potential with scan rate. The values of peak potentials were proportional to the logarithm of the scan rate for scan rates higher than 6.6 Vs^{-1} (Fig. 3B). The slope of the ΔE_c vs. log(v), was about, 68.5 mV. Using the equation $E_p = K - 2.3030(RT/\alpha nF)$ log v and the two electrons transferred for FAD, a charge transfer coefficient, α=0.433,

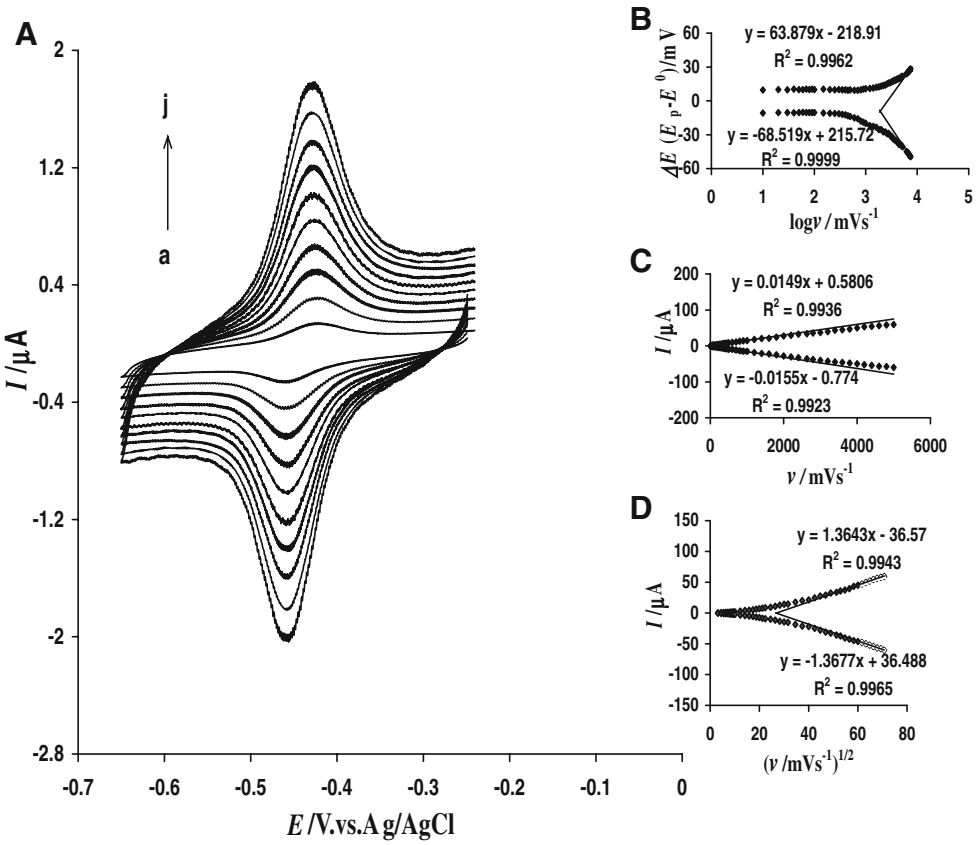

Fig. 3 **A** Cyclic voltammetric responses of a FAD/NiOx-modified GC electrode in pH 7 PBS at different scan rates, from inner to outer; 10, 20, 30, 40, 50, 60, 70, 80, 90, and 100 mVs^{-1}. **B** Variation of peak potential vs. log *v*. **C** and **D** Plots of peak currents vs. scan rate and square root of scan rate

was obtained. Introducing this α value in the following equation [39];

$$\log k_s = \alpha\log(1-\alpha) + (1-\alpha)\log\alpha - \log(\mathrm{RT}/nFv) - \alpha(1-\alpha)nF\,\Delta E/2.3RT \qquad (2)$$

An apparent surface electron transfer rate constant, k_s=63±0.1 s^{-1}, was estimated. This value is higher than reported value of (k_s) for immobilized FAD onto electrodeposited cobalt oxide nanostructure, 0.8±0.1 s^{-1} [25]. The large value of the electron transfer rate constant indicates a high ability of nickel oxide nanoparticles for promoting electrons between FAD and the electrode surface.

Interaction study of FAD with nickel oxide

The interaction of NiOx nanoparticles with FAD was studied using UV and FT-IR spectroscopy techniques. Figure 4 shows recorded UV spectra for indium tin oxide electrode modified with nickel oxide nanoparticles (Fig. 4, spectrum c), FAD (spectrum b), and nanocomposite containing FAD-NiOx. As shown, the coordination of N-7 to Ni(II) (Scheme 1) resulted in the increase of intensity of the 295 nm component (spectrum c) [35].

FT-IR has also used for investigation the interaction between FAD functional groups and nickel oxide nanoparticles. The recorded FT-IR spectra for FAD, NiOx, and FAD-NiOx is shown in Fig. 5. The wave number at 948 and 1,042–1,108 cm^{-1} are due to the presence of P-O-C and P-O-H links of the organic phosphorous groups on the nickel oxide [40, 41]. After adsorption of FAD onto nickel oxide nanoparticles, the intensity of proposed peaks decreased. Characteristic changes in the transmittance at the region 1,040–1,110 cm^{-1} indicate the phosphorous interaction during adsorption on nickel oxide. Furthermore, the appearance of new peak at 995 cm^{-1} and disappearance of the band at 948 cm^{-1} indicate the formation of nickel phosphate after adsorption. The peak at 1576 cm^{-1} attributed to the N-H bending shifts to the lower peak at 1530 cm^{-1} after immobilized onto nickel oxide.

XRD was used for characterization of NiOx crystallinity (supplementary file). No peaks corresponding to nickel oxide was observed, indicating that the NiOx film showed amorphous nature [42].

Stability and pH dependence of the FAD/NiOx-modified electrode

The stability of the GC/NiOx/FAD-modified electrode was examined by continuous potential cycling between −0.25 and −0.65 V in 0.1 M phosphate buffer solution (pH 7; Fig. 6A). As shown, no appreciable changes (less than 4%)

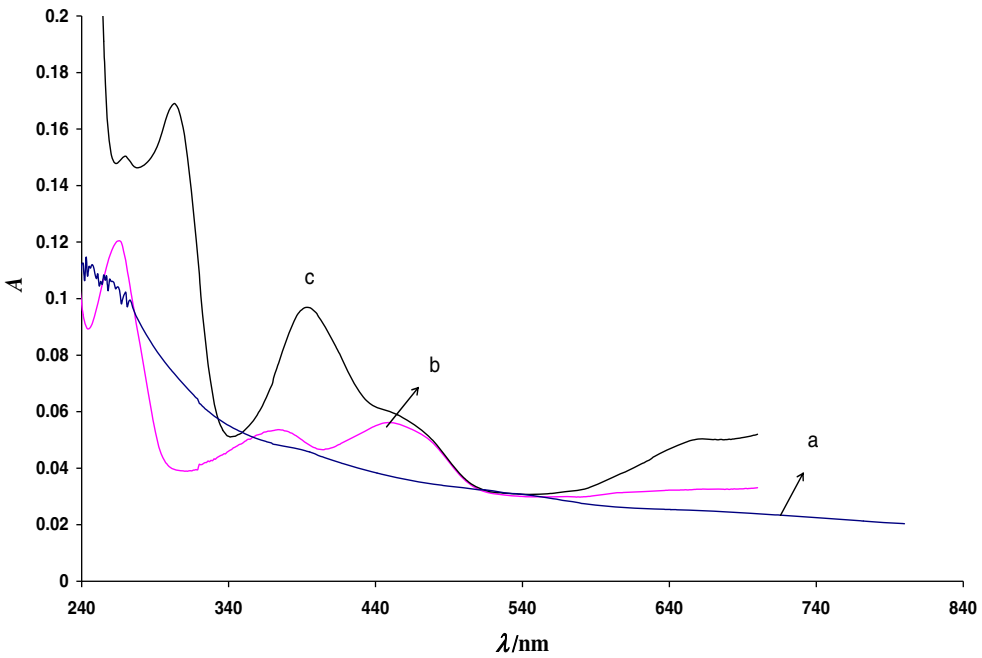

Fig. 4 UV–vis spectra of **a** NiOx, **b** FAD, and **c** FAD adsorbed onto NiOx

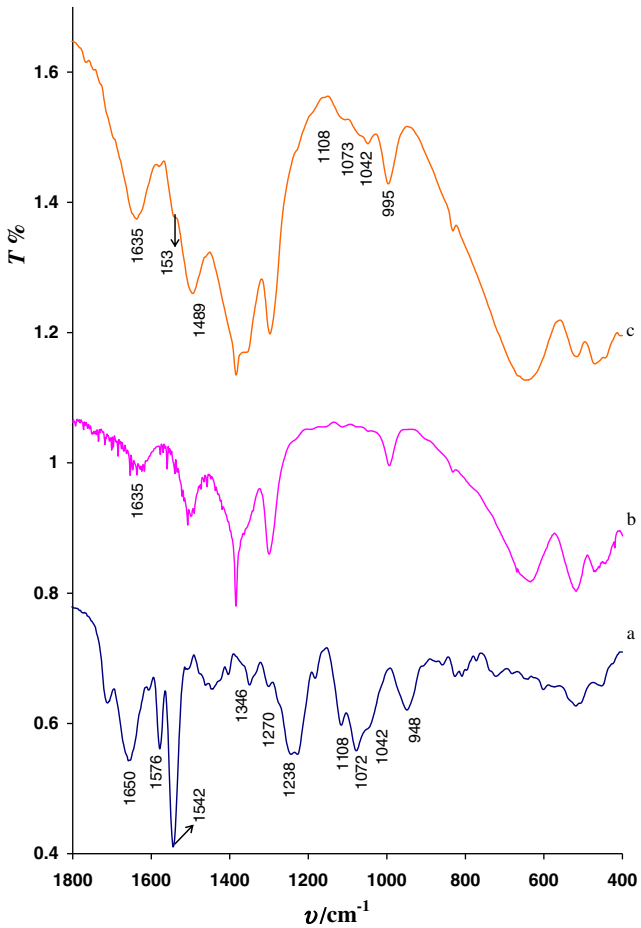

Fig. 5 FT-IR spectra of **a** FAD, **b** NiOx, and **c** FAD adsorbed onto NiOx

observed either in the peak current or the peak potential values after 200 cycles. In addition, it was found that the current value is decreased only by 9% when the electrode was immersed in buffer solution (pH 7) for 28 h (Fig. 6B). The stability of the modified electrodes was evaluated by the same method in electrolyte solutions at pH 2 and 10. The results indicated that the modified electrode was stable in acidic and alkaline solution. Since the method of electrode preparation is simple and fast (less than 10 min), the current decay is not a serious disadvantage for this modified electrode. The high stability of adsorbed FAD against desorption in aqueous solution is related to the chemical and mechanical stability of the NiOx film and the strong adsorption of FAD on the surface of nickel oxide nanoparticles. For investigating the effect of pH on the redox response of modified electrodes, cyclic voltammograms of the FAD/NiOx/GC electrode at various pH values were recorded. Figure 6C explains that the film exhibited a single redox couple in the pH range 2<pH<10. The value of $E^{o'}$ depended on the pH of the buffer solution. The inset of Fig. 6C illustrate the formal potential of the FAD/nickel oxide film plotted against the pH. The gradient was 58.6 mV/pH, a value close to that expected using the Nernst equation for a two-electron and two proton redox process. The pH response was due to the proton transfer from FAD to $FADH_2$.

Electrocatalytic reduction of $S_2O_8^{2-}$ on FAD/nickel oxide nanoparticles-modified GC electrode

Due to chemical stability, electrochemical reversibility, and high electron transfer rate constant of FAD at the NiOx

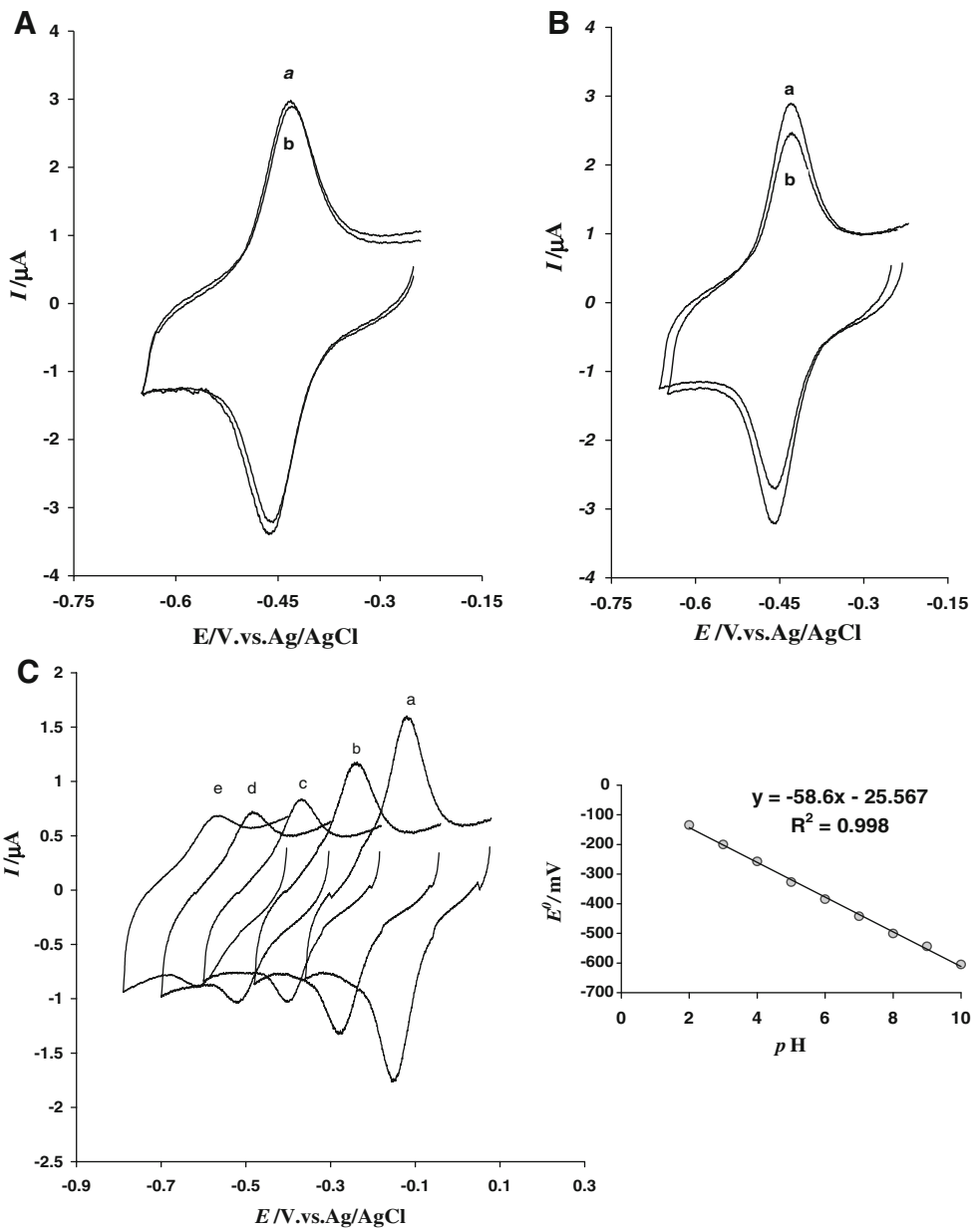

Fig. 6 **A** The first (*a*) and 200th (*b*) cyclic voltammograms of the FAD/NiOx-modified GC electrode in pH 7 PBS; **B** cyclic voltammogams of nano-NiOx/FAD-modified GC PBS, pH 7 (*a*); (*b*) as (*a*) after immersing the modified electrode for 28 h in PBS pH 7, scan rate 150 mVs^{-1}. Cyclic voltammetric response of the FAD/NiOx-modified GC carbon electrode at different pH (from right to left), 2,4,6,8, and 10 (*from right to left*); scan rate 50 mVs^{-1}. *Inset* shows the variation of standard potentials vs. pH values

nanoparticles-modified glassy carbon electrode, it can be used as a mediator to shuttle electron between electrodes and analyte molecules. Since the sulfur compounds play key roles in a number of pathways and biogeochemical processes, the determination of sulfur oxoanions is important for medicine, industry and environment [43, 44]. To evaluate the electrocatalytic activity of the FAD/NiOx composite film toward $S_2O_8^{2-}$ reduction, cyclic voltammograms of modified electrode in the absence and presence of $S_2O_8^{2-}$ were obtained (Fig. 7A, voltammograms "c and d"). As shown, when $S_2O_8^{2-}$ was added to buffer solution, reduction response started at −0.055 V and an obvious catalytic reduction peak appeared at the potential of −0.15 V (voltammogram "d"). For NiOx-modified GC electrode, no redox response for persulphate reduction can be seen in the potential range from 0.10 to −0.3 V (voltammogram "b"). The reducing of overvoltage and increasing the peak current of $S_2O_8^{2-}$ reduction confirm that FAD has high catalytic ability for $S_2O_8^{2-}$ reduction. Therefore, FAD immobilized onto NiOx nanoparticles are suitable as mediators to shuttle electron between $S_2O_8^{2-}$ and working electrode and facilitate electrochemical regeneration following electron exchange with $S_2O_8^{2-}$. In order to study the pH effect on the catalytic behavior of the modified electrode, the effect of the pH on the reduction of $S_2O_8^{2-}$ was examined over the pH range 2–10. A decrease in the reduction current density for $S_2O_8^{2-}$ is observed as the solution pH increase from 2 up to 10. Thus, the pH 2 is chosen as an optimum value pH for electro catalytic reduction of $S_2O_8^{2-}$. Cyclic voltammograms of the modi-

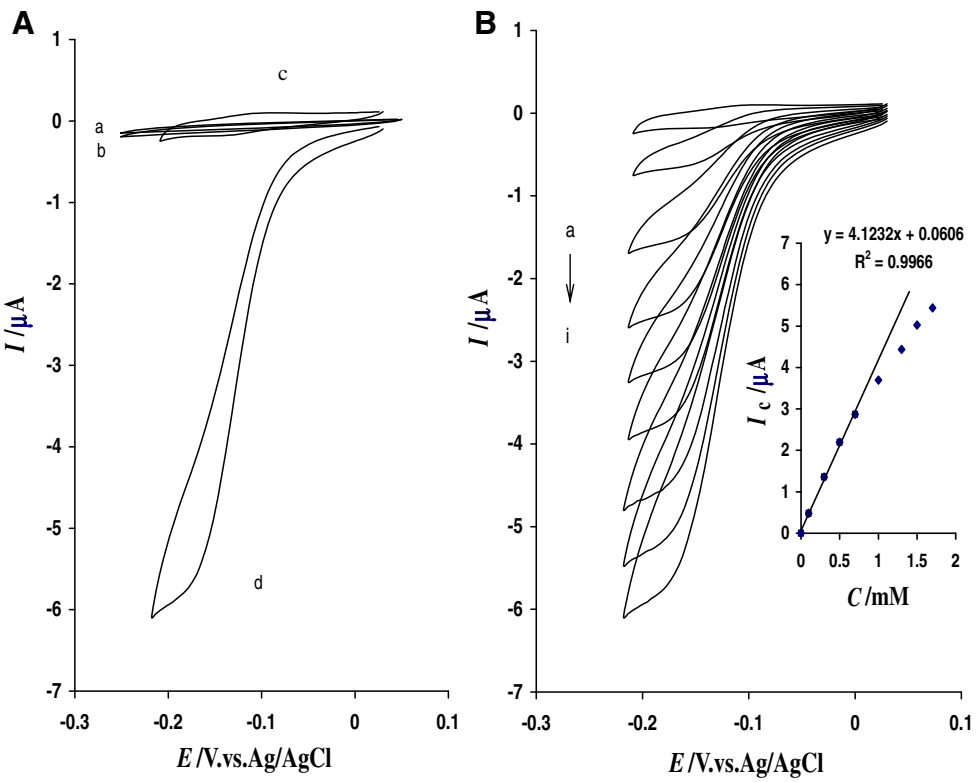

Fig. 7 **A** Recorded cyclic voltammograms of nano-NiOx-modified GC electrode in PBS (pH 2) at scan rate 20 mVs^{-1} (*a*); (*b*) as (*a*) in the presence 0.1 mM $S_2O_8^{2-}$. (*c* and *d*) as (*a* and *b*) for FAD/NiOx-modified GC electrode. **B** Cyclic voltammograms of FAD/NiOx-modified GC electrode in PBS (pH 2) at scan rate 20 mVs^{-1} in the presence of different concentrations of $S_2O_8^{2-}$ (from "a" to "i") : 0, 0.1, 0.3, 0.5,0.7, 1, 1.3, 1.5, and 1.7 mM; *Inset* plot of catalytic peak currents (I_c) vs. $S_2O_8^{2-}$ concentration

fied electrode in the presence different concentrations of $S_2O_8^{2-}$ were recorded (Fig. 7B). Inset of Fig. 7B shows the plot of catalytic current (at potential −0.15 V) vs. $S_2O_8^{2-}$ concentration. As shown, peak current linearly increased with an increase in the concentration of $S_2O_8^{2-}$ and the calibration plot is linear (correlation coefficient, 0.9966) for low concentrations (0.1–1.20 mM). The sensitivity and the detection limit (3σ) of the sensor towards $S2O8^{2-}$ were found to be 4.123 μA mM^{-1} and 10 μM, respectively. The cyclic voltammograms of modified electrode in buffer solution containing $S_2O_8^{2-}$ at different scan rates were recorded (Fig. 8). The peak current for the reduction of

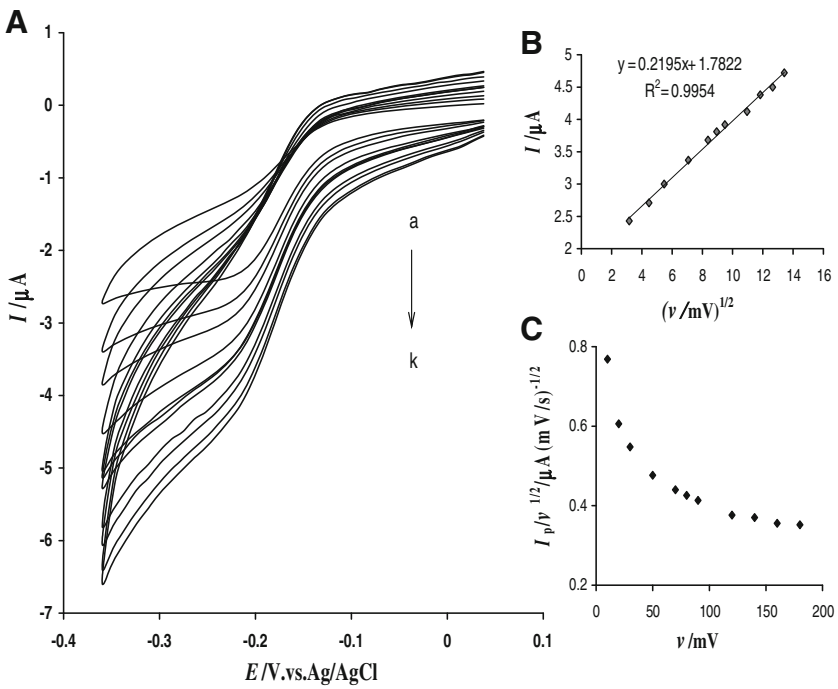

Fig. 8 Cyclic volttammetry response modified GC electrode in pH 2 PBS at buffer solution containing 0.3 mM of $S_2O_8^{2-}$ at different scan rates of (*from inner to outer*) 10,20,40,60,70,80,120,140,160, and 180 mVs^{-1}. **B** Plot of peak current vs. $v^{1/2}$. **C** Plot of $I_p/v^{1/2}$ vs. *v*

$S_2O_8^{2-}$ is proportional to the square root of the scan rate, suggesting that the process is controlled by diffusion as expected for a catalytic system. It can also be noted that by increasing the sweep rate the peak potential for the catalytic reduction of $S_2O_8^{2-}$ shifts to more negative values suggesting a kinetic limitation in the reaction between the redox sites of FADH2 and $S_2O_8^{2-}$. Also, a plot of the scan rate-normalized current ($Ip/v^{1/2}$) vs. scan rate (Fig. 8B) exhibited the characteristic shape of a typical *EC′* catalytic process [45]. Based on the obtained results, the following catalytic scheme describes the reaction sequence in the reduction of oxidation of $S_2O_8^{2-}$ with $FADH_2$.

$$FAD + 2e^- + 2H^+ \rightarrow FADH_2 \quad (3)$$

$$FADH_2 + S_2O_8^{2-} \xrightarrow{k_{cat}} FAD + 2H^+ + 2SO_4^{2-} \quad (4)$$

In order to get the information about the rate-determining step, a Tafel plot was drawn using the data derived from the rising part of the current–voltage curve recorded at scan rates 10 and 20 mVs^{-1} for solution containing 0.5 mM of $S_2O_8^{2-}$. A plot of potential vs. $\log_{10}$ (current) produced the value of 150.6 mV per decade, indicating that one electron process was involved in the rate-limiting step, assuming a charge transfer coefficient of α=0.70. Under the above conditions for an *EC′* mechanism, the Andrieux and Saveant theoretical model [46] can be used in order to calculate the catalytic rate constant. Based on this theory, we have the following relation between the peak current and the concentration of substrate compound for the case of slow scan rates and large catalytic rate constant;

$$I_p = 0.446nFAD^{1/2}C_s(vF/RT)^{1/2} \quad (5)$$

where D and C_s are the diffusion coefficient (1.15×10^{-5} cm^2s^{-1}) [46], and the bulk concentration (mol cm^{-3}) of $S_2O_8^{2-}$, respectively, and other symbols have their usual meanings. Low values of *k*cat results in values of the coefficient lower than 0.496. For low scan rate (5–20 mV s^{-1}), the average value of this coefficient was found to be 0.12 for a FAD/NiOx-modified glassy carbon electrode with a coverage of 4.66×10^{-11} mol cm^{-2} and effective surface area (A) of 0.085 cm^2 in 0.1 mM $S_2O_8^{2-}$ at pH 2. According to the Andrieux and Saveant approach and using Fig. 1 of reference [46] (supplementary file), the average value of k_{cat} is 1 (±0.2)$\times10^4$ M^{-1} s^{-1}, is higher than catalytic rate constant of $S_2O_8^{2-}$ reduction $k_{cat} = 1.265\times10^3M^{-1}s^{-1}$ at lead pentacyano-nitrosylferrate-modified carbon ceramic electrode[47]. The high value of k_{cat} indicates high electro-catalytic activity of the sensor for $S_2O_8^{2-}$ detection. These results indicate high catalytic activity of the sensor for $S_2O_8^{2-}$ detection.

Amperometric determination of $S_2O_8^{2-}$ at FAD/NiOx-modified glassy carbon electrodes

Figure 9 shows a typical current–time response of the modified electrode for the continuous additions of 0.1 mM (A) and 3 μM (C) of $S_2O_8^{2-}$ to pH 2 PBS at an applied

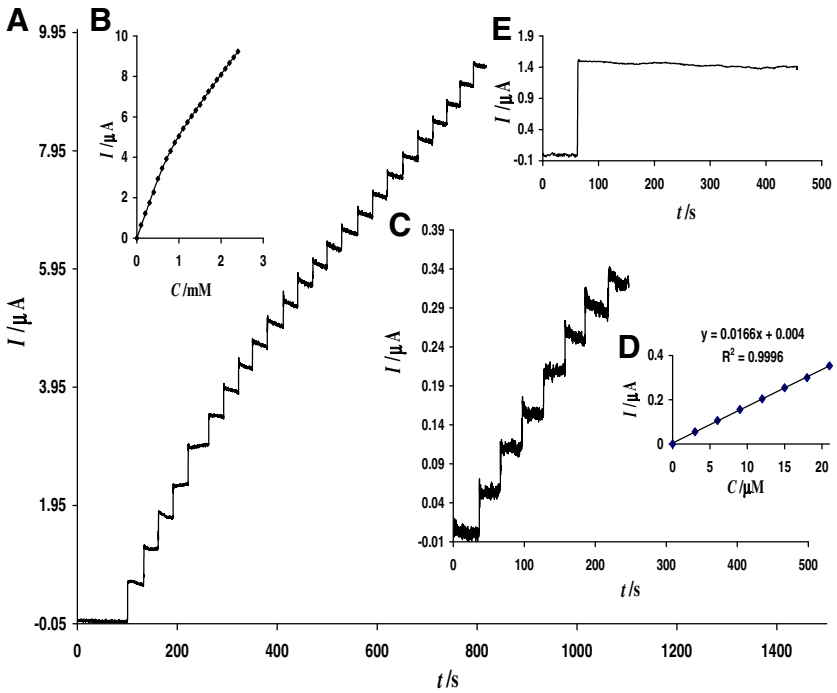

Fig. 9 Amperometric response of rotating FAD/NiOx-modified GC electrode (rotation speed 1,000 rpm)held at −0.20 V in buffer solution (pH 2) during successive addition of $S_2O_8^{2-}$ **A** 0.1 mM and **C** 3.0 μM $S_2O_8^{2-}$. *Insets* (**B** and **D**) are the plots of amperometric current vs. $S_2O_8^{2-}$ concentration and **E** chronoamperogram of modified electrode for 0.2 mM $S_2O_8^{2-}$ during a long time period, 500 s

potential of −0.2 V. As shown upon additions of $S_2O_8^{2-}$, the reduction current increased steeply to reach a stable value. The electrode achieved 95% of the steady-state current within 3 s indicating clearly that the electrocatalytic response was very fast. Figure 9b and d are the plots of response currents versus $S_2O_8^{2-}$ concentration. It can be observed that the response current is linear with the $S_2O_8^{2-}$ concentration in the range 3 μM–1.5 mM. As can be shown in Fig. 9, linear calibration curve over the range 3–21 μM (7 points) is: $I(\mathrm{mA}) = 0.0166\left[S_2O_8^{2-}\right](\mathrm{mM}) + 0.004\mathrm{mA}$, $R^2 = 0.9996$, indicating that the regression line is fitted very well with the experimental data and the regression equation can be applied in the unknown sample determination. The detection limit (signal to noise was 3) and sensitivity were 0.39 μM and 16.6 nA/μM, respectively, which is comparable or better than other electrochemical sensors for $S_2O_8^{2-}$ determinations [19, 44, 48]. The stability of the sensor was examined by amperometric detection and the sensor showed good long-term stability under continuous use. Figure 9e shows the amperometric response of 0.2 mM $S_2O_8^{2-}$ during prolonged 7.0-min experiment. As we can see, the response remains stable throughout the experiment (only 4% decrease in current was observed), indicating no inhibition effect of $S_2O_8^{2-}$ and its reduction products for modified electrode. The operation stability of the sensor was investigated in continuous operation mode. The storage stability was examined at the same modified electrode in 15 consecutive days. While not in use, the modified electrode was stored in 4°C in refrigerator. In the repeated measurements on the consecutive days, the sensor response for same $S_2O_8^{2-}$ concentration was maintained at 95% of the initial response. Therefore, the modified electrode has excellent, stable, and strong mediation properties and facilities the low potential amperometric measurement of $S_2O_8^{2-}$. The long-term stability of the modified electrode could be attributed to both structure stability of nanocomposite as well as the preparation process for modified method fabrication The selectivity of the sensor was also evaluated by determination of $S_2O_8^{2-}$ in the presence of common interfering ions such as, IO_3^-, ClO_4^-, NO_2^-, SO_3^{2-}, $S_2O_3^{2-}$, $S_2O_6^{2-}$, Ni^{2+}, Co^{2+}, and Zn^{2+}. Figure 10 shows amperometric response of the rotated modified electrode for $S_2O_8^{2-}$ in the presence of several interference in buffer solution, pH 2. As can be seen, no response is observed for modified electrode in the presence of different interfering substances. Furthermore, the electrode response for persulfate after adding interfering substances was not changed. The selectivity and the anti-interference advantages of the sensor are largely attributed to the low operating potential used in the determination.

Conclusion

In the present study, electrodeposited nickel oxide nanostructures were used for electrolees adsorption of FAD. Due to formation of stable complexes between phosphate and nitrogen of adenine group in FAD, it can be immobilized strongly on the NiOx nanomaterials. The immobilized FAD shows good stability and electrochemical reversibility at wide pH range due to their excellent biocompatibility of

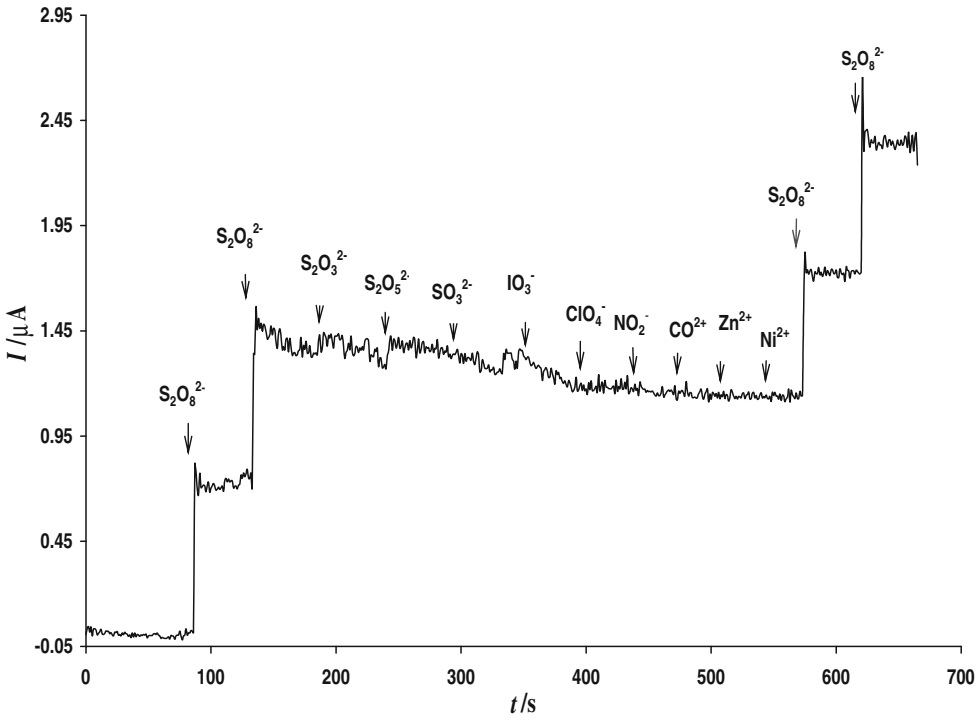

Fig. 10 Amperometric response of rotating FAD/NiOx-modified GC electrode (rotation speed 1,000 rpm) held at −0.20 V in buffer solution (pH 2) during successive addition of $S_2O_8^{2-}$ (0.2 mM) and 1 mM of IO_3^-, ClO_4^-, NO_2^-, SO_3^{2-}, $S_2O_6^{2-}$, $S_2O_3^{2-}$, Ni^{2+}, Co^{2+}, and Zn^{2+}

nickel oxide nanostructures. The modified electrode shows excellent electrocatalytic activity toward $S_2O_8^{2-}$ reduction at reduced overpotential. The resulting biosensor exhibits many advantages, such as high sensitivity, low detection limit, wide concentration range, good reproducibility, and storage stability. Detection limit, response time sensitivity, and linear concentration range of GC/NiOx/FAD-modified electrode were 0.38 μM, 3 s, 16.6 μA mM^{-1}, and 3 μM–1.5 mM, respectively. These analytical parameters are compared or better than reported values in literature using other based-modified electrodes. Owing to high biocompatibility, high adsorption ability, and little harm to the biological activity of nickel oxide nanomaterials, the composition these nanostructures and biomolecules may be favorable for construction of biosensors and bioelectronic devices.

Acknowledgment The financial support of Iranian Nanotechnology Initiative and Research Office of University of Kurdistan is gratefully acknowledged. We thank Dr. Roshan Khosnavazi for recording FT-IR spectra.

References

1. Lin KC, Chen SM (2005) J Electroanal Chem 578:213
2. Wang Y, Zhu G, Wang E (1997) Anal Chim Acta 338:97
3. Garjonyte R, Malinauskas A, Gorton L (2003) Bioelectrochem 61:39
4. Mc Garvey C, Beck S, Quach S, Birss VI, Elzanowska H (1998) J Electroanal Chem 456:71
5. Kama MM, Elzanowska H, Gaur M, Kim D, Birss VI (1991) J Electroanal Chem 318:349
6. Zhang J, Chi Q, Wang E, Dong S (1995) Electrochim Acta 40:733
7. Noll G, Kozma E, Grandori R, Carey J, Schodl T, Hauska G, Daub J (2006) Langmuir 22:2378
8. Gorton L, Johansson G (1980) J Electroanal Chem 113:151
9. Verhagen MFJM, Hagen WR (1992) 1992. J Electroanal Chem 334:339
10. Ivanova YN, Karyakin AA (2004) Electrochem Commun 6:120
11. Karyakin AA, Ivanova YN, Revunova KV, Karyakina EE (2004) Anal Chem 76:2004
12. Sagawara K, Kamiya N, Hirabayashi G, Kuramitz H (2006) Electroanalysis 18:1001
13. Kubota LT, Gorton L, Roddick-Lanzilotta A, McQuillan AJ (1998) Bioelectrochem Bioenerg 47:39
14. Alvarez NS, Castanon MJL, Ordieres AJM, Blanco PT (2005) Electroanalysis 17:445
15. Alvarez NS, Alvarez PS, Castanon MJL, Ordieres AJM, Blanco PT (2005) Anal Chem 77:4286
16. Chen SM, Liu MI (2006) Electrochim Acta 51:4744
17. Lin KC, Chen SM (2006) J Electroanal Chem 589:52
18. Kumar AA, Chen SM (2007) Sens Actuators B 123:964
19. Chen SM, Chzo WY, Thangamuthu R (2009) Electroanalysis 21:2331
20. Wakayama H, Hall SR, Mann S (2005) J Mater Chem 15:1134
21. Choy JH, Kwak SY, Park JS, Jeong YJ, Portier J (1999) J Am Chem Soc 121:1399
22. Ding L, Hao C, Xue Y, Ju H (2007) Biomacromolecules 8:1341
23. Ruiz-Hitzky E, Darder M, Aranda P (2005) J Mater Chem 15:3650
24. Kumar AS, Chen SM (2007) J Solid State Electrochem 11:993
25. Salimi A, Hallaj R, Mamkhezri H, Hosain SMT (2008) J Electroanal Chem 619–620:31
26. You T, Niwa, Chen O, Hayashi K, Tomita M, Hirono S (2003) Anal Chem 75:5191
27. Xing W, Li F, Yan Z, Lu GQ (2004) J Power Sources 134:324
28. Kamal H, Elmaghraby EK, Ali SA, Abdel-Hady K (2005) Thin Solid Films 483:330
29. Cosnier S (2000) Appl Biochem Biotechnol 89:127
30. Salimi A, Sharifi E, Noorbakhash A, Soltanian S (2006) Electrochem Commun 8:1499
31. Salimi A, Sharifi E, Noorbakhash A, Semnani A (2008) Biosens Bioelectron 24:792
32. Salimi A, Sharifi E, Noorbakhash A, Soltanian (2007) Biosens Bioelectron 22:3146
33. Moghaddam AB, Ganjali MR, Dinarvand R, Ahadi S, Saboury AA (2008) Biophys Chemist 134:25
34. Kaczmarek P, Bojczuk MJ, Bal W, Kasprzak KS (2005) J Inorg Biochem 99:737
35. Bojczuk MJ, Kaczmarek P, Bal W, Kasprzak KS (2004) J Inorg Biochem 98:1770
36. Salimi A, Roushani M, Hallaj R (2006) Electrochim Acta 51:1952
37. Giovanelli D, Lawrence NC, Jiang L, Jones TGL, Compton RG (2003) Sens Actuators B 88:320
38. Brown AP, Anson FC (1997) Anal Chem 49:1589
39. Laviron E (1979) J Electroanal Chem 101:19
40. Panda GC, Das SK, Bandopadhyay TS, Guha AK (2007) Colloids Surf B Biointerfaces 57:135
41. Viladkar S, Agarwal R (1996) Bull Chem Soc Jpn 69:95
42. Kandalkar SG, Gunjakar GL, Lokhande CD (2008) Appl Surf 254:5540
43. Miller PL, Vasudevan D, Gschwend PM, Roberts AL (1998) Environ Sci Technol 32:1269
44. Guo W, Xu L, Xu B, Yang Y, Sun Z, Liu S (2009) J Appl Electrochem 39:647
45. Pariente E, Lorenzo E, Tobalina F, Abruna HD (1995) Anal Chem 67:3936
46. Andrieux CP, Saveant JM (1978) J Electroanal Chem 93:163
47. Thomberg T, Lust E (2000) J Electroanal Chem 485:89
48. Razmi H, Heidari H (2008) Electroanalysis 21:2370